

DeepTrace: Learning to Optimize Contact Tracing in Epidemic Networks with Graph Neural Networks

Chee Wei Tan, Pei-Duo Yu, Siya Chen and H. Vincent Poor

Abstract—Digital contact tracing aims to curb epidemics by identifying and mitigating public health emergencies through technology. Backward contact tracing, which tracks the sources of infection, proved crucial in places like Japan for identifying COVID-19 infections from superspreading events. This paper presents a novel perspective of digital contact tracing as online graph exploration and addresses the forward and backward contact tracing problem as a maximum-likelihood (ML) estimation problem using iterative epidemic network data sampling. The challenge lies in the combinatorial complexity and rapid spread of infections. We introduce *DeepTrace*, an algorithm based on a Graph Neural Network (GNN) that iteratively updates its estimations as new contact tracing data is collected, learning to optimize the maximum likelihood estimation by utilizing topological features to accelerate learning and improve convergence. The contact tracing process combines either BFS or DFS to expand the network and trace the infection source, ensuring comprehensive and efficient exploration. Additionally, the GNN model is fine-tuned through a two-phase approach: pre-training with synthetic networks to approximate likelihood probabilities and fine-tuning with high-quality data to refine the model. Using COVID-19 variant data, we illustrate that *DeepTrace* surpasses current methods in identifying superspreaders, providing a robust basis for a scalable digital contact tracing strategy.

Index Terms—Digital contact tracing, Contagion source detection, Maximum likelihood estimation, Graph neural network, Online graph exploration

I. INTRODUCTION

Since the onset of the COVID-19 pandemic, a multitude of mobile applications [1]–[4] have been deployed to detect individuals potentially exposed to the SARS-CoV-2 coronavirus and mitigate its transmission. These applications offer exposure notifications as an adjunct to conventional contact tracing methodologies, which are often resource-intensive and time-consuming. Utilizing network science-based data analytics and machine learning, these solutions show promise in automating widespread coverage, crucial for monitoring the rapid spread of infectious diseases and their variants [5]. The goal of digital contact tracing is thus to diminish the spread of the epidemic, but this is complicated by factors such as the speed of disease

spreading, asymptomatic infections, and the infectiousness characteristics, i.e., a few superspreaders affecting the whole (e.g., approximately 20% of infected individuals responsible for 80% of transmissions [6]). Designing robust digital contact tracing automated by network science and machine learning is still in its infancy.

It has been recently shown that [2], [7]–[9] compared with ‘forward’ tracing (i.e., to whom disease spreads), ‘backward’ tracing (from whom disease spreads) can be more effective due to overlooked biases arising from the heterogeneity in contacts. Tracing sources of spreading (i.e., backward contact tracing), as had been used in Japan [8], has proven effective as going backward can pick up infections that might otherwise be missed at superspreading events. The ability to identify the source of spreading (i.e., the Patient Zero or superspreaders in a pandemic) is essential to contact tracing. In this paper, we formulate a jointly forward and backward contact tracing problem that leverages the maximum likelihood estimation as a subproblem to design contact tracing algorithms based on a network centrality design approach.

A. Related Works

The contagion source inference problem was first studied in the seminal work [10] as a maximum likelihood estimation problem based on a Susceptible-Infectious (SI) model [11], which is a special case of the classical susceptible-infected-recover (SIR) model in epidemiology [12]–[14]. This problem becomes challenging when dealing with a very large graph, as the sheer scale amplifies the intricacy of tracking numerous spreading likelihoods across its vast network, compounding the complexity of calculating permissible permutations for each node. For the degree-regular tree special case, this problem can be solved in polynomial time by a network centrality approach, i.e., the *rumor centrality* [10], [15], which is proportional to the number of permitted permutations. Equivalently, this optimal likelihood estimate is the graph centroid [16]–[18]. The network centrality approach [10] has been extended to scenarios like random trees [19], [20], multiple snapshot observations [21], multiple sources [22] and the *epidemic centrality* for a disease pandemic in [23]. Unlike the snapshot model [10], other studies [24]–[27] use time series data, Bayesian analysis and stochastic processes to solve the contagion source inference problem via sequential and quickest detection techniques. For a comprehensive overview of the work on the detection of contagion sources, we refer the reader to [18].

However, computing the ML estimator for the source on large epidemic networks can be computationally challenging

C. W. Tan is with Nanyang Technological University, Singapore, Nanyang Ave., Singapore (e-mail: cheewei.tan@ntu.edu.sg).

P. D. Yu is with the Department of Applied Mathematics, Chung Yuan Christian University, Taiwan (e-mail: peiduoyu@cycu.edu.tw).

S. Chen is with the Department of Computer Science, City University of Hong Kong, Hong Kong (e-mail: siyachen4-c@my.cityu.edu.hk).

H. V. Poor is with the Department of Electrical and Computer Engineering, Princeton University, Princeton, NJ 08544 USA (e-mail: poor@princeton.edu).

This work is supported in part by the U.S. National Science Foundation under RAPID Grant IIS-2026982, the Ministry of Science and Technology of Taiwan under Grant 110-2115-M-033-001-MY2, Hong Kong ITF Project ITS/188/20 and an Institute for Pure and Applied Mathematics fellowship.

[10], [23], particularly as the network size grows and complexity increases with the presence of cycles. Thus, using Graph Neural Networks (GNNs) becomes a viable option. Various studies have used GNNs for pandemic control [28]–[31]. Gatta [28] focuses on estimating epidemiological model parameters, differing from other works [29]–[31] that aim to identify patient zero (superspreaders). Shah [29] examines SIR and SEIR models with graph convolutional networks, but these are limited to “transductive” settings, unable to handle graph inputs of varying sizes. On the other hand, the work in [30] also considers the same discrete time SIR spreading model, but in the training dataset of this paper, susceptible nodes were pre-assigned values such that susceptible nodes are unlikely to be the source estimator using external expert knowledge. For both works [29], [30], the label of each piece of data in the training set is the source of the outbreak but not the ML estimator of the source according to their spreading model. Thus, the labels used in previous works do not have statistical significance; sometimes, the source may not equal the ML estimator, which introduces noise into the training data.

To address the issues related to the training set [29], [30], and the computational complexity challenges discussed in [15], [23], we propose a GNN-based framework with a two-phase semi-supervised training approach. In this framework, we use graphs that contain the ML estimator for the superspreader during the fine-tuning phase. Specifically, we adopt the SI spreading model, as thoroughly studied in [15], [18], [23]. It has been established that the ML estimator is equivalent to certain network centers [10], [17], [23]. This equivalence allows us to easily obtain high-quality labeled data for specific network topologies, thereby improving the accuracy of identifying the most likely superspreader.

Lastly, our previous work [31] serves as a pilot study on using GNNs for backward contact tracing, framing contact tracing as online graph exploration. Compared to the conference version, we have studied the performance of the DFS strategy (cf. Lemma 1 and Theorem 2). Additionally, Theorem 3 demonstrates the feasibility of using GNNs to *learn to optimize* maximum likelihood estimators in graphs. In our experimental simulations, we have included numerous tests, evaluating the DFS and BFS strategies combined with various source detection methods from the literature across different network topologies.

B. Main Contributions

- We frame digital contact tracing as an online graph exploration problem, where backward contact tracing is solved as a maximum likelihood estimation problem that captures the dynamic effects of the pandemic’s spread over time. This iterative process involves a challenging nonconvex optimization problem. We tackle this using modified graph neural networks to predict network centrality measures. Applied to epidemic networks of varying sizes, our low-complexity algorithm, DeepTrace, progressively refines the prediction of the most likely source of contagion as more data becomes available.
- We utilize GNNs to perform the task of backward contact tracing. By training the GNN to learn to optimize

the maximum likelihood estimation (MLE) problem, we enhance its ability to solve the complex nonconvex optimization task of identifying the contagion source. We integrate network centrality methods from the literature for calculating MLE for the source to generate high-quality training data, thereby improving the efficiency and accuracy of our GNN training.

- For the forward contact tracing component, we employed graph theory and algorithmic analysis to thoroughly examine the differences between BFS and DFS strategies. Our experimental simulations demonstrated that using BFS to expand the epidemic network enables faster detection of superspreaders compared to the DFS strategy.
- Using data sets of both synthetic epidemic networks and contact tracing data during the COVID-19 pandemic in Taiwan and Hong Kong, we demonstrate that Algorithm DeepTrace outperforms the state-of-the-art heuristics in [10], [23].

II. CONTACT TRACING PROBLEM FORMULATION

Let us first introduce the spreading models including one relevant to COVID-19 in [14] and then present the digital contact tracing optimization problem formulation followed by its mathematical analysis.

A. Epidemic Spreading Model

There are numerous models in the literature in the study of the spread of infectious diseases ranging from commonly well-known ones like the Susceptible-Infectious (SI) model to the Susceptible-Infectious-Recovery-Susceptible (SIRS) models [12]–[14], [24]. Despite being the most basic one, the SI model can accurately model a pandemic in its early stage (e.g., COVID-19 ca. 2020), whereas other SIRS models [14] incorporate complex factors like virus mutation, societal response (e.g., mask wearing and social distancing) and the use of vaccines (e.g., COVID-19 ca. 2021).

We focus primarily on the SI model for analysis and use the more accurate COVID-19 model [14] for numerical performance evaluation. The SI model assumes that there are only two types of individuals, say susceptible and infectious during the epidemic spreading. Also, we follow the assumption that the times between infection events are independent and exponentially distributed [15] with an average infection time (with most estimates of COVID-19 incubation period ranging from 1 to 14 days [14]). The virus spreads in a social contact network can be modeled by a diffusion process on a graph denoted by \mathbb{G} . Let $V(\mathbb{G})$ and $E(\mathbb{G})$ denote the set of nodes and edges in \mathbb{G} , which represent people and their social contacts (an edge exists between two persons if, say, they are within 6 feet for more than 15 minutes) respectively. We shall call \mathbb{G} the *underlying network*, where the topology of \mathbb{G} poses a constraint to the epidemic spreading [15], [23], [32]. The spreading of the virus starts from a node in \mathbb{G} (i.e., the superspreader) and spreads to other nodes under the constraint that a susceptible node can be infected only if at least one of its neighboring nodes has been infected. At some point in time, all infected nodes in \mathbb{G} form a connected subgraph of

\mathbb{G} , denoted as \mathbb{G}_N and is called the *epidemic network*, where N represents the number of nodes in the epidemic network.

This epidemic network \mathbb{G}_N and the infection spreading dynamics are assumed to be unknown to a contact tracer, and this is the chief uncertainty faced by all contact tracers, who therefore adopt a strategy to collect this data starting from an index case (i.e., the first documented infected person) and trace his or her close contacts (according to the topology of \mathbb{G}) and so on.

B. Forward and Backward Contact Tracing

At various stages of contact tracing, we model an instantaneous snapshot of a subgraph of \mathbb{G}_N that we call the *contact tracing network*. This contact tracing network grows by one (infected) node at each stage. If the traced node is infected, we continue to trace the node's neighbors; otherwise, we stop tracing along a path involving this node. Let G_n denote the contact tracing network with n nodes at the n -th stage of tracing (thus the index case is G_1), hence we have $G_n \subseteq \mathbb{G}_N \subseteq \mathbb{G}$. A goal of contact tracing is to find the node in \mathbb{G}_N that is most likely to be the superspreader, as shown in Fig. 1. However, this most-likely superspreader may not yet be in G_n , meaning that the contact tracing effort is still in its early stage or not fast enough (relative to the pandemic spreading speed). In such a case, backward contact tracing should yield an estimate as close as possible to this most-likely superspreader. In other words, given the available data at the n -th stage, the contact tracer finds the node in G_n that is the fewest number of hops away from the most-likely superspreader in \mathbb{G}_N (i.e., the optimal maximum likelihood estimate had this \mathbb{G}_N been given entirely upfront to the contact tracer [10]).

Given the data G_n harvested by contact tracing at the n -th stage, we have the following maximum-likelihood estimation (MLE) problem:

$$\hat{v} \in \arg \max_{v \in G_n \subseteq \mathbb{G}_N \subseteq \mathbb{G}} \mathbb{P}(G_n | v), \quad (1)$$

where $\mathbb{P}(G_n | v)$ is the likelihood function and \hat{v} is the most-likely superspreader of the current observed G_n . The key challenge is that \mathbb{G}_N is unknown to the contact tracer who has to consider:

Forward contact tracing: How to construct the contact tracing network efficiently starting from a given index case?

Backward contact tracing: How to solve (1) to give the best instantaneous estimate of the superspreader given the data?

Answering both the forward and backward contact tracing jointly constitutes an iterative statistical inference process to track the most likely superspreader in the entire epidemic network. Specifically, for the forward contact tracing subproblem, it is natural to enlarge the forward contact tracing network with breadth-first search (BFS) or depth-first search (DFS) graph traversal starting from the index case. For the backward contact tracing subproblem, let us suppose that a given node v in G_n is the superspreader. Then, starting from this particular node, there are a number of possible ways to infect all the other nodes consistent with the given graph G_n harvested by contact tracing at the n -th stage. Even though \mathbb{G}_N is unknown,

it is reasonable for a contact tracer to assume a possible infection order in G_n by a *permitted permutation* given as $\sigma = \{v_1 = v, v_2, \dots, v_n\}$. Thus, we can reformulate problem (1) as:

$$\hat{v} \in \arg \max_{v \in G_n} \sum_{\sigma \in \Omega(G_n | v)} \mathbb{P}(\sigma | v), \quad (2)$$

where $\Omega(G_n | v)$ is the collection of all permitted permutations for G_n rooted at v , and $\mathbb{P}(\sigma | v)$ is the probability of the permitted permutation σ with v as source. Under the SI spreading model used in [10], [15], [23], the probability of a susceptible node being infected in the next time period is uniformly distributed among all outreaching edges from the infected nodes at the boundary of G_n , and the probability of a permitted permutation is as follows:

$$\mathbb{P}(\sigma | v) = \prod_{i=1}^{n-1} \frac{\Phi_i}{\sum_{j=1}^i [d(v_j) - 2\Phi_{j-1}]}, \quad (3)$$

where $d(v_i)$ is the degree of node v_i in \mathbb{G} , and $\Phi_i = |e(v_{i+1}) \cap (\bigcup_{j=1}^i e(v_j))|$ with $e(v_i)$ being the set of edges connecting to node v_i . For the edge case, we define $\Phi_0 = 0$. The value of Φ_i counts the number of edges linked between node v_{i+1} and its infected neighbors. Hence, the probability of being infected is proportional to the number of infected neighbors. Note that the probability defined in (3) also works if \mathbb{G} is a graph with multiple edges, i.e., the number of edges between a given pair of nodes can be more than one.

If \mathbb{G} is a general tree as a special case, then every newly infected node, say v_{i+1} only connected to one of the infected nodes; otherwise, \mathbb{G} is not a tree. Hence, when \mathbb{G} is a general tree, we have $\Phi_i = 1$, for $i \neq 0$, and the probability of a permitted permutation can be given by [10]:

$$\mathbb{P}(\sigma | v) = \prod_{i=1}^{n-1} \frac{1}{\sum_{j=1}^i d(v_j) - 2(i-1)}. \quad (4)$$

C. Regular Trees and General Graphs

In this section, we will discuss the differences in using maximum likelihood estimation to find the source estimator when the underlying network is a regular tree versus a general graph. Additionally, we will explore how the known results for regular trees can be applied to general graphs.

From (3), we can observe that when \mathbb{G} is a regular tree, both Φ_i and $d(v_i)$ are constants which implies the value of (3) is also a constant. Thus, the computation of the likelihood only depends on the value of $|\Omega(G_n, v)|$ in (2), which simplifies the computation. On the other hand, it is still unknown whether there exists an efficient method for calculating the likelihood when \mathbb{G} is a general graph since $\mathbb{P}(\sigma | v)$ is different for each possible $\sigma \in \Omega(G_n, v)$ and the size of $\Omega(G_n, v)$ grows exponentially with n . To overcome this computational complexity issue, our goal is to leverage GNN to find the MLE. Various theoretical results on regular trees or unicyclic regular graphs [10], [23] provide us a way to generate high quality dataset, the label of each piece of data is the exact MLE of the epidemic graph, for training GNN. Moreover, the analysis in Theorem 1, 2 shows the best and the worst possible outcomes

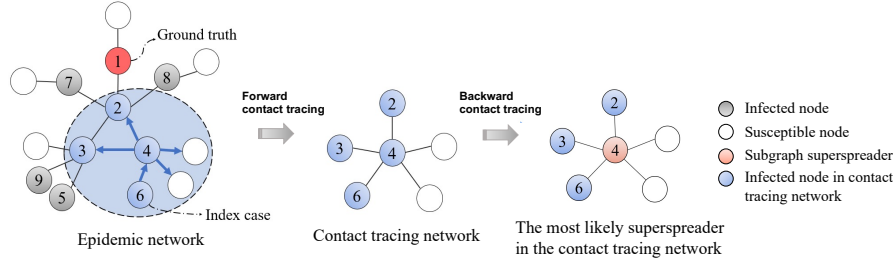


Fig. 1: Illustration of an epidemic network \mathbb{G}_9 with nine infections (shaded nodes) whose numbering indicates the infection order starts from the ground truth, i.e., the real superspreader. The contact tracing network G_4 (within a dotted circle) starts from the index case node v_6 (blue arrows show the tracing directions) by forward contact tracing. The backward contact tracing is to find the node in \mathbb{G}_9 that is most likely to be the superspreader.

during the contact tracing on regular trees, which provides us reasonable bounds on the performance of the contact tracing on general graphs.

Coming back to the contact tracer starts from the index case G_1 and collects more data in a forward manner (i.e., enlarging G_n in (2)), the contact tracer also predicts the superspreader for that instant by solving (1). Intuitively, this means that as the contact tracing subgraph G_n grows, the contact tracer desires this prediction to be closer (in terms of the number of hops in \mathbb{G}_N) to the most likely superspreader in \mathbb{G}_N . Taking this into account, how should G_n grow in size in *forward contact tracing*? We propose to enlarge G_n using the BFS and the DFS graph traversal algorithms [33], [34], which is described in detail in the next section.

III. DIGITAL CONTACT TRACING BY BFS AND DFS

In this section, we detail interesting insights into tracing superspreaders in BFS tracing networks (using BFS traversal for forward contact tracing) and DFS tracing networks (using DFS traversal for forward contact tracing). Mathematically, the forward contact tracing process yields a rooted tree \mathbb{G}_N , whose nodes help solve (2). For special cases, Theorem 1 states that this maximizer of (2), i.e., the graph centroid of \mathbb{G}_N , converges to the graph centroid of \mathbb{G}_N along a simple path on \mathbb{G}_N when N is fixed.

A. Contact Tracing by Breadth-First Search

Firstly, we propose to enlarge \mathbb{G}_N using the BFS graph traversal algorithm [33], [34]. Fig. 2 illustrates this with a tracer who starts from node v_a and then moves to node v_d (the most likely superspreader) gradually.

Let $\text{dist}(u, v)$ denote the graph distance (i.e., number of hops) between node u and node v . If N is fixed, then we have the following result showing that $\text{dist}(v_n^*, v_N^*)$ is a decreasing sequence as n grows when \mathbb{G}_N is a d -regular tree, where d -regular tree is a tree that all non-leaf nodes have d neighbors.

Theorem 1: If \mathbb{G} is a d -regular tree, and there exists a node \bar{v} such that for any two leaf nodes v_{leaf} and u_{leaf} in \mathbb{G}_N ,

$$|\text{dist}(v_{\text{leaf}}, \bar{v}) - \text{dist}(u_{\text{leaf}}, \bar{v})| \leq 1, \quad (5)$$

then the trajectory of v_n^* is exactly the shortest path from the index case v_1^* to v_N^* in \mathbb{G}_N .

Theorem 1 implies that in the special case where \mathbb{G} is a d -regular tree, the epidemic network \mathbb{G}_N satisfies (5). By employing the BFS contact tracing strategy, we can progressively

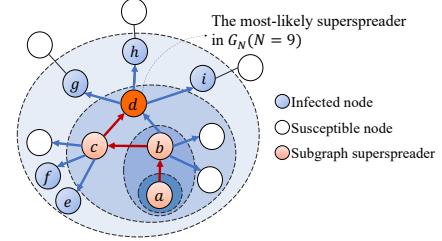


Fig. 2: As the contact tracing network enlarges starting from the index case v_a with BFS traversal, as ordered alphabetically $\{a, b, c, \dots, i\}$, the most likely superspreader given by (2) moves closer (in terms of number of hops) to the most-likely superspreader v_d in the epidemic network \mathbb{G}_N (indicated by red arrows).

approach the optimal solution v_N^* with each expansion of G_n . Thus, Theorem 1 underscores the effectiveness of the BFS strategy in achieving optimal solutions.

Next, we provide an example, a class of graph structure satisfying (5). If G_n is a complete N -ary tree, then $|\text{dist}(v_{\text{leaf}}, v_n^*) - \text{dist}(u_{\text{leaf}}, v_n^*)| \leq 1$ for every v_{leaf} in G_n . Then, from Theorem 1, we have that the trajectory of v_n^* is exactly the shortest path from v_1^* to v_N^* in \mathbb{G}_N .

B. Contact Tracing by Depth-First Search

Now, let us consider enlarging \mathbb{G}_N with DFS tracing strategy [34], which is illustrated in Fig. 3. We can categorize all consecutive pairs (v_i^*, v_{i+1}^*) in S into the following three types:

$$\begin{aligned} S_1 &= \{(v_i^*, v_{i+1}^*) | v_i^* = v_{i+1}^*\}, \\ S_2 &= \{(v_i^*, v_{i+1}^*) | v_i^* \neq v_{i+1}^*, \text{ and } v_j^* \neq v_{i+1}^*, \forall j < i\}, \\ S_3 &= \{(v_i^*, v_{i+1}^*) | v_i^* \neq v_{i+1}^* \text{ and } v_j^* = v_{i+1}^* \text{ for some } j < i\}. \end{aligned}$$

The first type of consecutive pairs in S_1 represent the estimated superspreader that remains the same when the contact tracing network grows from G_i to G_{i+1} . The second type, S_2 implies that the node v_{i+1}^* is computed as the estimated superspreader for the first time. The third type, S_3 implies that v_{i+1}^* had been chosen as the estimated superspreader before. Since the contact tracing network is a subgraph of a degree-regular tree, there are two maximum likelihood estimators when \mathbb{G}_N can be divided into two subgraphs with the same size [15]. We assume for each consecutive pair (v_i^*, v_{i+1}^*) in S_2 and S_3 , we have $P(G_{i+1} | v_{i+1}^*) > P(G_{i+1} | v_i^*)$, i.e., we only select v_{i+1}^* as the new estimator when $P(G_{i+1} | v_{i+1}^*) >$

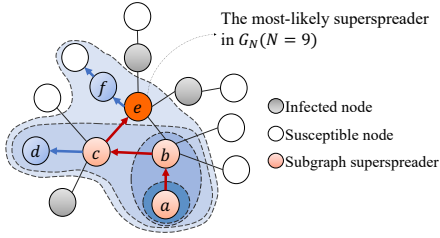


Fig. 3: As the contact tracing network enlarges starting from the index case v_a with DFS traversal, as ordered alphabetically $\{a, b, c, \dots, f\}$, the most-likely superspreader given by (2) moves closer (in terms of number of hops) to the most-likely superspreader v_e in the epidemic network \mathbb{G}_N (indicated by red arrows).

$P(G_{i+1} \mid v_i^*)$. Let $|S_1|$, $|S_2|$, and $|S_3|$ denote the size of these three types of consecutive pairs, respectively. Let T^v be a rooted tree of \mathbb{G}_N rooted at v and denote the subtree of T^v rooted at u as T_u^v . Note that the size of S is N , so there are only $N - 1$ consecutive pairs in S . Moreover, S_1, S_2 and S_3 are mutually exclusive. Hence, we can conclude that

$$|S_1| + |S_2| + |S_3| = N - 1. \quad (6)$$

We introduce the following insights of the sequence S by considering S_1 , S_2 , and S_3 .

Lemma 1: Let \mathbb{G} be a d -regular tree, and we apply the DFS tracing strategy, then we have $|S_1| \geq |S_2| \geq |S_3|$. Moreover, we can bound $|S_1|$, $|S_2|$ and $|S_3|$ as follows:

- $|S_1| \geq (N - 1)/2 \geq |S_2|$,
- $|S_3| \leq (N - 1)/4$.

The edge cases of Lemma 1 happen when \mathbb{G}_N is a line graph with an odd number of nodes, and the index case is either the center or the leaf node of \mathbb{G}_N . We can deduce that more than half of those consecutive pairs in S are type one, i.e., the estimated superspreader will remain the same most of the time. Lastly, this lemma serves as a tool when proving the following theorem.

Theorem 2: Let \mathbb{G} be a d -regular tree and we apply DFS tracing strategy, if $v \in \mathbb{G}_N$ and $(\cdot, v) \in S_3$, then we have $|(\cdot, v)| \leq \log_2(N)$, where $|(\cdot, v)|$ denote the number of the pair (\cdot, v) in S_3 .

Theorem 2 implies that when using the DFS tracing strategy to build the contact tracing network, each node in the epidemic network \mathbb{G}_N should not be identified as the superspreader more than $\log_2(N)$ times as the contact tracing network expands iteratively.

Next, let us compare the performance of both the DFS and BFS contact tracing strategies using two quantifiable metrics (that can be readily measured once the ground truth is given). The first metric is the average error, which is defined by

$$\frac{1}{N} \sum_{i=1}^N \text{dist}(v_i^*, v_N^*). \quad (7)$$

The second metric is the first detection time, which is the time when the estimated most-likely superspreader first matches the ground truth and is defined as

$$\min\{i \mid v_i^* = v_N^*\}. \quad (8)$$

The average error metric assesses the performance of any digital contact tracing algorithm, accounting for the selected forward contact tracing strategy and potential suboptimality in maximizing likelihood estimates. On the other hand, the first detection time measures how quickly the contact tracing algorithm can zoom in on identifying the most-likely superspreader without a global view of the overall epidemic networks. It is desired that the most-likely superspreader is the actual ground truth even as the epidemic networks size N increases independently of the digital contact tracing effort.

It is not surprising that the performance of any forward contact tracing strategy depends on the distance between the index case and the most-likely superspreader, i.e., $\text{dist}(v_1^*, v_N^*)$. For example, let the epidemic network \mathbb{G}_{10} be a 3-regular tree with six leaves. Assume that the index case is a leaf node, then the pair (average error, first detection time) is $(0.7, 6)$ and $(0.8, 7)$ for the DFS and BFS strategies, respectively. However, if the index case is exactly the ground truth, then the pair (average error, first detection time) should be $(0.4, 0)$ and $(0, 0)$ for the DFS and BFS strategies, respectively. If N is fixed and \mathbb{G}_N has a sufficiently small graph diameter, the convergence of the BFS strategy may be slower than that of the DFS strategy because the initial sets of nodes may have more neighbors. On the other hand, when \mathbb{G}_N has a sufficiently large graph diameter, the DFS strategy may converge slower than the BFS strategy. Other graph-theoretic features of \mathbb{G}_N , such as degree and cycles, can also affect the choice of the forward contact tracing strategy.

C. Interpretation as Online Maze Solving

Interestingly, the above technique to decompose (1) into the respective forward and backward contact tracing subproblems can be interpreted as solving a maze where the epidemic network \mathbb{G}_N induces an abstract maze topology. *Each step taken by the maze solver corresponds to the discovery of a leaf node v^n of the rooted tree \mathbb{G}_N at the n th iteration of the forward contact tracing stage and a corresponding v_n^* of the backward contact tracing.* We can treat two aforementioned sequences $S = (v_1^*, v_2^*, \dots, v_N^*)$ and $X = (v^1, v^2, \dots, v^N)$ as two trajectories on two mazes respectively. The trajectory S is to find the desired exit v_N^* and the trajectory X traverses the graph. However, these two mazes are explored and solved at the same time, i.e., once the maze solver takes a step from v^i to v^{i+1} , there is a corresponding movement on S from v_i^* to v_{i+1}^* . If we assume that there is only one contact tracer, and each time a new node is discovered in the $(i + 1)$ th iteration, the contact tracer has to travel from v^i to v^{i+1} with the distance $\text{dist}(v^i, v^{i+1})$. Then, the goal of the contact tracing is to minimize both the total traveling distance $\sum_{i=1}^n \text{dist}(v^i, v^{i+1})$ of the contact tracer and the first detection time of v_N^* (i.e., the optimal maximum-likelihood estimate had \mathbb{G}_N been given in advance) during the discovery of all infected nodes in \mathbb{G}_N . The maze solver (i.e., contact tracer) knows neither the complete maze topology induced by \mathbb{G}_N nor the target v_N^* . Upon visiting a vertex (i.e., the graph centroid of \mathbb{G}_N) in this abstract maze for the first time, the maze solver has information about some of its incident edges only. The contact tracer has a map of

all the infected nodes visited and edges connecting them, but cannot tell where each leads until \mathbb{G}_N is fully traversed.

Forward contact tracing and backward contact tracing are thus analogous to the process of online maze exploration and maze traversal. Let us connect the aforementioned results on forward contact tracing with this abstract maze interpretation: suppose a given abstract maze is a tree, and there is no cost for each newly discovered node, then Theorem 1 illustrates that the BFS traversal yields the shortest path (i.e., shortest sequence of centroids) to solving the maze, and Theorem 2 describes that the DFS traversal yields a sequence of steps with less variance between steps (i.e., consecutive centroids having least hop distances). In fact, if \mathbb{G}_N is a tree, this particular abstract maze constructed using graph centroids will be topologically identical to one constructed by using either the rumor centrality or the distance centrality by virtue of the fact that the graph centroid is equivalent to the rumor center and the distance center [17].

As the maze analogy emerges from the network centrality perspective of solving (1), further insights into its theoretical computational complexity can be gained by linking it to the classical topic of online graph exploration, involving online sequential decision-making to determine which destinations can be reached and when [35], [36]. In particular, the corresponding offline problem for online graph exploration is the Traveling Salesman Problem which has NP-hard complexity. This means that finding the optimal solution of (1) in an online setting is, in general, even NP-hard to approximate. The state-of-the-art online algorithm (also based on a generalization of Depth First Search) has a constant competitive ratio of 16 for planar undirected graphs [35], [36]. This abstract maze-solving perspective can thus open promising avenues for contact tracing, utilizing either low-complexity greedy algorithms or more advanced algorithmic designs.

More importantly, machine learning techniques can offer new insights to *learn to optimize* this class of problems in a scalable manner. There are recent works in [37], [38] that used GNN to address online graph exploration as a reinforcement learning problem. In solving (1) online with access to local information, the maze solver builds a complete map of the topology of the abstract maze of graph centroids and, in addition to BFS and DFS traversal, can leverage other maze-solving algorithms in the literature, e.g., Tremaux’s algorithms and the A* search algorithm [34]. It is possible to adapt different horizons of forward contact tracing steps to adapt the topological space of this abstract maze and to give weights to its edges. There are also new possibilities to construct the underlying abstract maze by considering different measures of network centrality that can inspire novel jointly optimal forward and backward contact tracing strategies to solving (1).

IV. DEEPTRACE: LEARN TO OPTIMIZE TRACING

In general, solving the NP-hard problem in (2) is computationally challenging, especially when the underlying \mathbb{G}_N is large and with N increasing throughout the contact tracing process. To address this challenge, we leverage GNNs to propose a scalable contact tracing algorithm, named DeepTrace

(see Section IV-B), capitalizing on the above forward and backward contact tracing decomposition. DeepTrace aims to emulate the online graph exploration strategy to maximize the number of previously unseen unique states in a limited number of steps by employing a graph-structured memory to encode the past trajectory of the contact tracer and hidden structures in the spreading model and network topologies.

A. Deep Learning on Graphs

As a deep learning model for processing unstructured data, a GNN extracts graph features and information from the input data that are encoded as graphs. The learning mechanism of the GNN is to iteratively aggregate features and information from neighboring nodes for each node in the input graphs. Aggregating information from neighbors is equivalent to a message-passing process among nodes in a graph. Lastly, we update the values of the learning parameters for regression or classification tasks [39], [40]. To effectively capture both the statistical and graph topology attributes inherent in network-structured input data, the training stage of the GNN in semi-supervised machine learning is crucial. Specifically, the equations (3) and (4) can act as node label generators during the construction of fine-tuning datasets for our proposed Algorithm DeepTrace (see Section IV-C2).

To apply GNNs to solve (2), we need to consider two key computational aspects: the underlying epidemic network \mathbb{G}_N is unknown to the contact tracer, and the size of \mathbb{G}_N can be potentially massive. The role of the GNN is therefore to facilitate the computation of a (possibly suboptimal) solution to (2) when \mathbb{G}_N is large. Due to the adaptability of GNNs, we can first generate a training set using small graphs (e.g., tens or hundreds of nodes) that are subgraphs of \mathbb{G}_N and augment the descriptors with the structural features for each individual node of these graphs as the input data. The training stage requires that correct labels (that is, exact values of (3) be associated with each of these small graphs. As the size of the graph grows, the computational cost of (3) becomes expensive. We can instead approximate (3) by sampling method to efficiently compute labels for training data. Finally, we train the GNN model with the input subgraph data iteratively to update the neural network hyperparameters, as shown in Fig. 4. We explain this GNN architecture and its training in the following.

B. Algorithm DeepTrace: Pre-training and Fine-tuning GNNs

In this section, we propose to solve the problem (2) for backward contact tracing in the epidemic network \mathbb{G}_N by using GraphSage [40], a popular inductive GNN model, which can be adapted to different network size. To obtain the contact tracing network \mathbb{G}_N , we construct our GNN model using the LSTM [41] aggregator that aggregates information from the neighbors of a node and the element-wise mean [41] to combine the local information of a node with the aggregated information. We define the l th layer of the GNN as follows:

$$\begin{aligned} \mathbf{h}_{N_{\mathbb{G}_N}(v)}^{(l)} &= \text{LSTM}(\{\widehat{\mathbf{w}}^{(l-1)}, \mathbf{h}_u^{(l-1)} : u \in N_{\mathbb{G}_N}(v)\}), \\ \mathbf{h}_v^{(l)} &= \max(0, \widetilde{\mathbf{w}}^{(l)} \cdot [\mathbf{h}_v^{(l-1)}; \mathbf{h}_{N_{\mathbb{G}_N}(v)}^{(l)}]), \end{aligned} \quad (9)$$

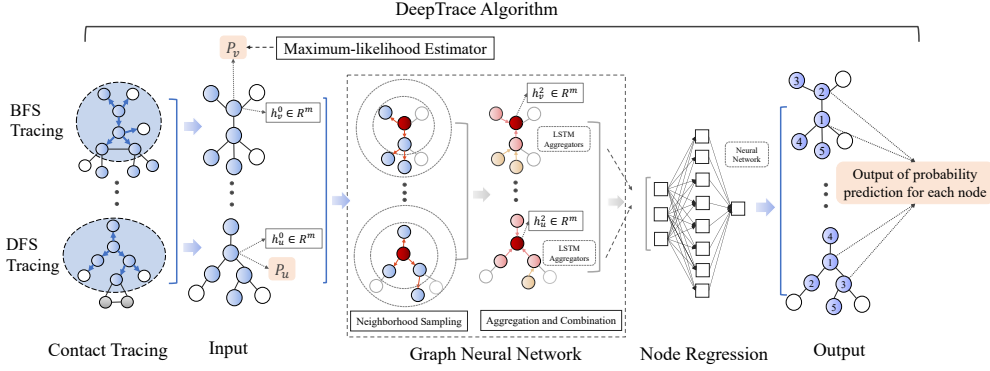


Fig. 4: The overall architecture of Algorithm DeepTrace employs a GNN, taking as input several small-scale networks obtained through BFS and DFS methods. Each node in these networks has structural features and a training label representing the permitted permutation probability. Semi-supervised learning is conducted using GraphSage with LSTM aggregators.

where $\hat{\mathbf{w}}^{(l)}$ and $\check{\mathbf{w}}^{(l)}$ are the learning parameters in the LSTM aggregators and combination function, respectively. The initial node feature vector is $\mathbf{h}_v^{(0)} = [\mathbf{1}, \hat{r}(v), \check{r}(v)]^T$ for $v \in \mathbb{G}_N$, which we discuss in the Section IV-D. We first prove the effectiveness of backward contact tracing with the GNN model (9) in the following result.

Theorem 3: For a given epidemic network $\mathbb{G}_N = (V, E)$, denote $\text{diam}(\mathbb{G}_N)$ as the diameter of \mathbb{G}_N , and define each layer of the GNN model by (9). Then for $\forall \epsilon > 0$ there exist a parameter setting $(\hat{\mathbf{w}}^*, \check{\mathbf{w}}^*)$ in (9) with at most $L = \text{diam}(\mathbb{G}_N) + 1$ layers such that

$$|\mathbf{h}_v^{(L)} - \mathbb{P}(\mathbb{G}_N | v)| < \epsilon, \forall v \in V.$$

Based on the classic result on the learning capability of feedforward neural networks [42], Theorem 3 states that the value of $\mathbb{P}(G_n | v)$ can be approximated by GNNs with at most $\text{diam}(\mathbb{G}_N) + 1$ layers within an arbitrary error ϵ . From an algorithm design perspective, Theorem 3 establishes the feasibility of approximating $\mathbb{P}(G_n | v)$ using GNNs, providing the theoretical foundation for our subsequent approach to learning $\mathbb{P}(G_n | v)$ with GNNs.

Since obtaining labeled datasets for training (9) is computationally challenging, we employ a two-phase semi-supervised training approach to tune the learning parameters in (9): a pre-training phase followed by a fine-tuning phase. In the pre-training phase, we train the GNN in DeepTrace using a dataset of contact tracing networks with approximations of $\mathbb{P}(G_n | v)$ as labels for each node. This dataset can be easily obtained, as described in the Section IV-C. This pre-trained GNN exhibits a great enhancement in performance when compared to a GNN with randomly initialized learning parameters. Then, in the fine-tuning phase, we proceed to adjust the learning parameters in the pre-trained model using an additional dataset of contact tracing networks that contain the exact values of $\mathbb{P}(G_n | v)$ as labels for each node in the networks. This dataset can include special cases of regularly-sized networks, such as d -regular graphs [10], [17], as well as a small number of contact tracing networks that have the exact values of $\mathbb{P}(G_n | v)$ obtained by calculating probabilities of all the permitted permutations in (2) as labels for each node. Acquiring the latter dataset requires more effort and

is considered highly valuable. Therefore, it is not wasted on training the GNN from scratch, but rather for fine-tuning the pre-trained model to further enhance its accuracy. This two-phase training process enables us to effectively utilize both the dataset with approximate values of $\mathbb{P}(G_n | v)$ and the dataset with exact values of $\mathbb{P}(G_n | v)$. Thus, we can attain a GNN that exhibits enhanced performance while reducing the time and computational resources required for training. We then apply the fine-tuned models to contact tracing graphs of different scales. This leads to our GNN-based learning algorithm, which we call *Algorithm DeepTrace* as described below.

As contact tracing progresses, Algorithm 1 ultimately identifies the superspreaders for the entire epidemic network. The computational complexity of contact tracing in Algorithm 1 can be decomposed into three main components: sampling complexity, aggregation complexity, and the complexity of the final regression layer. Suppose there are N nodes in the epidemic network. During the sampling procedure, the GNN samples a fixed-size neighborhood for each node. If each node samples S neighbors and this process is repeated for L layers, then the total number of nodes sampled for each node is $O(S^L)$. Consequently, the sampling complexity for contact tracing the entire epidemic network is $O(N^2 S^L)$. For the aggregation procedure, the GNN aggregates information from its neighbors sampled. Assume that the feature dimension is m . Since the LSTM aggregator processes the features of the sampled neighbors, the complexity of the aggregation step is $O(mS^2)$ per node per layer. Thus, the aggregation complexity for contact tracing the entire epidemic network is $O(N^2 L m S^2)$. Regarding the final regression layer in the GNN, a fully connected layer is used to map the node embeddings to the target values, i.e., the maximum likelihood of being superspreaders, of the nodes. Given that the output dimension is 1, the complexity for each node is $O(m)$. Therefore, the complexity of the final regression layer for tracking the contact throughout the epidemic network is $O(N^2 m)$. Overall, the computational complexity of the contact tracing in Algorithm 1 is $O(N^2 L m S^2)$.

Algorithm 1: DeepTrace

Input: The index case (i.e., G_1); the GNN model defined in (9) with randomly initialized parameters and contact tracing data.

Output: The likelihood probability for every node in the network to be the contagion source.

Training:

1. Pre-train the GNN model using contact tracing networks with node labels as the approximations of $\tilde{\mathbb{P}}(G_n|v)$ in (11).
2. Fine-tune the GNN model using contact tracing networks with node labels having the exact values of $\mathbb{P}(G_n|v)$ in (1).

Prediction:

3. **for** $n = 2$ **to** N **do**
 - Generate the contact tracing network G_n using either the BFS or DFS search strategy at the n -th stage;
 - Construct the node features $\mathbf{h}_v^0 = [\mathbf{1}, \hat{r}(v), \check{r}(v)]^T$ for each node in G_n ;
 - Predict the source probability for each node in G_n using the fine-tuned GNN model in Step 2;
- end**
-

C. Training Process with Semi-supervised Learning

To train the GNN model in DeepTrace during the two-phase training process, we define the loss functions for the pre-training and fine-tuning phase, respectively, as follows:

$$L_p(\hat{\mathbf{w}}, \check{\mathbf{w}}, v \mid v \in G_n) = \sum_{v \in G_n} |\log(\tilde{\mathbb{P}}(G_n \mid v)) - \mathbf{h}_v^{(L)}(\hat{\mathbf{w}}, \check{\mathbf{w}})|^2,$$

and

$$L_f(\hat{\mathbf{w}}, \check{\mathbf{w}}, v \mid v \in G_n) = \sum_{v \in G_n} |\log(\mathbb{P}(G_n \mid v)) - \mathbf{h}_v^{(L)}(\hat{\mathbf{w}}, \check{\mathbf{w}})|^2,$$

where $\tilde{\mathbb{P}}(G_n \mid v)$ is the approximation of $\mathbb{P}(G_n \mid v)$, $\hat{\mathbf{w}} = (\hat{\mathbf{w}}^{(1)}, \dots, \hat{\mathbf{w}}^{(L)})$ and $\check{\mathbf{w}} = (\check{\mathbf{w}}^{(1)}, \dots, \check{\mathbf{w}}^{(L)})$. We take the logarithm of the likelihood probabilities to avoid arithmetic underflow, as the values of likelihood probabilities can be extremely small as the infected network grows in size.

Next, we describe how to construct the training data sets for pre-training and fine-tuning the GNN model, respectively.

1) *Data Annotation for Pre-training:* For the labeled training data in the pre-training phase, we can use an approximate estimator of (1) to efficiently obtain $\tilde{\mathbb{P}}(G_n \mid v)$ for each node v in the epidemic networks, minimizing time and effort. When the epidemic networks are degree-irregular trees, the ML estimator in (1) aims to calculate the sum of all probabilities of permitted permutations. We can rewrite (1) as follows:

$$v \in \arg \max_{v \in G_n} \bar{\mathbb{P}}(G_n \mid v) |\Omega(G_n \mid v)|, \quad (10)$$

where $\bar{\mathbb{P}}(G_n \mid v)$ is the average of the probabilities of all permitted permutations. We can calculate $|\Omega(G_n \mid v)|$

using a message-passing algorithm from [43] with a time complexity of $\mathcal{O}(N)$. However, obtaining the exact value of $\bar{\mathbb{P}}(G_n \mid v)$ is challenging, as it requires identifying all the permitted permutations of \mathbb{G}_N and their corresponding probabilities. Therefore, we randomly select a small sample of the permitted permutations, denoted by $\tilde{\Omega}(G_n \mid v)$, and approximate $\bar{\mathbb{P}}(G_n \mid v)$ by averaging their probabilities. Thus, the approximate MLE problem is formulated as follows:

$$\begin{aligned} \hat{v} &\in \arg \max_{v \in G_n} \frac{1}{|\tilde{\Omega}(G_n \mid v)|} \sum_{\sigma \in \tilde{\Omega}(G_n \mid v)} \mathbb{P}(\sigma \mid v) |\Omega(G_n \mid v)| \\ &= \arg \max_{v \in G_n} \tilde{\mathbb{P}}(G_n \mid v). \end{aligned} \quad (11)$$

2) *Data Annotation for Fine-tuning:* Since we already have a preliminary GNN model from pre-training, we can further refine it using a small amount of high-quality data. Specifically, this involves using data from epidemic networks with exact likelihood probabilities assigned to each node. To construct a piece of labeled data with exact likelihood probability for fine-tuning, a natural idea is to calculate the likelihood probability of each node directly by using (3) or (4). We first generate an epidemic network \mathbb{G}_N with N nodes, then for each node $v \in \mathbb{G}_N$ we generate all permitted permutation $\sigma \in \Omega(\mathbb{G}_N \mid v)$ starting from v and compute $\sum_{\sigma \in \Omega(G_n \mid v)} \mathbb{P}(\sigma \mid v)$ using (3). Furthermore, we can construct data samples for which exact likelihood probabilities are easily obtainable using (4), such as the d -regular tree. In this case, since the probabilities of all permitted permutations are identical, it is evident from (10) that the likelihood probability for a node in a d -regular tree, as given by (2), is proportional to the epidemic centrality in [17], which can be computed using the message-passing algorithm described in [17].

D. Construction of Node Features

To ensure the effectiveness of GNN learning for solving (2) in *Algorithm DeepTrace*, it is crucial to meticulously design the node features. This careful design enables the extraction of node information from the underlying epidemic network \mathbb{G}_N , which corresponds to a specific spreading model during the training phase. We now consider several node features such as the proportion of instantaneously infected nodes, and boundary distances within the graph. Notably, constructing these features requires only linear computational complexity, $\mathcal{O}(N)$, as illustrated in Fig. 5.

Infected proportion: This is the ratio of the number of infected neighbors of a node v_i to the number of all its neighbors:

$$\hat{r}(v_i) = \frac{\hat{d}(v_i)}{d(v_i)},$$

where $\hat{d}(v_i)$ is the number of infected neighbors of the node v_i . For example, the number of infected neighbors of nodes v_1, v_2, v_3, v_4 , and v_5 in Fig. 5 are 1, 1, 4, 1 and 1, leading to an infected proportion of nodes v_1, v_2, v_3, v_4 , and v_5 being $\frac{1}{2}, \frac{1}{3}, 1, \frac{1}{3}$, and $\frac{1}{4}$, respectively. This feature is to represent each node's ability to infect new individuals. Intuitively, a node with a lower infected proportion has a higher probability of

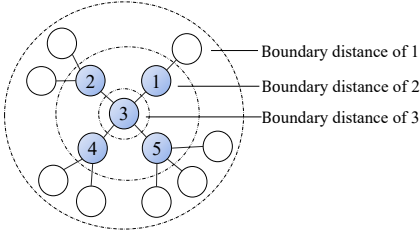


Fig. 5: An example of a given epidemic network illustrating the boundary distance for each node.

infecting new individuals and a smaller probability of being the source. Moreover, this particular node feature aims to capture the effect of the particular node position in the permitted permutation in (3). A node with a lower infected proportion tends to be located at the front of the permitted permutation order, resulting in a smaller permutation probability. For example, as in Fig. 5, the different positions of Node 5 for the permitted permutation $\{3, 1, 2, 4, 5\}$ and $\{5, 3, 1, 2, 4\}$ result in a probability of 1.7857×10^{-3} and 1.0204×10^{-3} , respectively.

Boundary distance ratio: As the infectivity of the virus evolves over time—newly symptomatic infectors generally exhibit higher infectivity, whereas long-term symptomatic infectors display lower infectivity—we assume that nodes at the boundary of the epidemic network are newly symptomatic infectors, while those further from the boundary are long-term symptomatic infectors. This characteristic is captured by the boundary distance ratio feature, which is the ratio of the shortest distance from the node v_i to the farthest leaf node at the network boundary, as shown in Fig. 5, and is denoted by

$$\check{r}(v_i) = \frac{b(v_i)}{\max_{v_j \in G_n} b(v_j)},$$

where $b(v_j)$ is the boundary distance of node v_j . For example, the boundary distances of node v_1, v_2, v_4 and v_5 in Fig. 5 are 2, and the boundary distances of node v_3 is 3, so that the boundary distance ratio of nodes v_1, v_2, v_3, v_4 and v_5 are $\frac{2}{3}, \frac{2}{3}, 1, \frac{2}{3}$ and $\frac{2}{3}$, respectively. Notice that we grow G_i using tree traversal algorithms; hence G_i can be treated as a tree, and the boundary distance ratio of each node in G_i is well-defined. From (2), we see that finding the source also requires information on the size of the collection of all permitted permutations $\Omega(G_n | v)$. Notice that a node with a larger boundary distance ratio tends to have a larger collection of permitted permutations. For example, there are 24 permitted permutations when we choose node v_3 to be the source, but only 6 permitted permutations if we choose either node v_1, v_2, v_4 or v_5 to be the source.

V. PERFORMANCE EVALUATION

In this section, we first provide simulation results on the performance of the approximate ML estimator (11). Secondly, we compare the BFS and DFS strategies by simulating the procedure of forward and backward contact tracing. Lastly, we demonstrate the effectiveness of *Algorithm DeepTrace* on both synthetic networks and real-world networks based on COVID-19 contact tracing data in Hong Kong and Taiwan. As

mentioned in Section I-A, the methods proposed in [29], [30] are based on the assumptions of either SEIR or SIR spreading model which is different from the SI model considered in this paper. We thus focus on baseline comparison relevant to the SI model, namely the rumor center heuristic in [15] and the SCT (Statistical Distance-Based Contact Tracing) algorithm in [23]. The software implementation of *Algorithm DeepTrace* and data used in our experiments can be found in <https://github.com/convexsoft>.

A. DeepTrace for Synthetic Networks

Data size	Nodes	Edges	Labels	Task
500	50~1000	49~999	$\log(\mathbb{P}(G_n v))$	Pre-training
250	≈ 50	≈ 50	$\log(\mathbb{P}(G_n v))$	Fine-tuning
250	50~1000	49~999	$\log(\mathbb{P}(G_n v))$	Testing

TABLE I: The summary of the datasets of the synthetic epidemic networks for pre-training, fine-tuning and testing when training the GNN in DeepTrace.

We evaluate the performance of *Algorithm DeepTrace* in identifying superspreaders within epidemic networks using a two-phase semi-supervised learning approach, comprising a pre-training phase and a subsequent fine-tuning phase. To begin with, we generate 1000 synthetic epidemic networks, including Erdős Rényi random graphs, Barabási-Albert random graphs, Watts-Strogatz random graphs, and random regulars, SBM networks and sensor networks [44], as training datasets for the GNN model in *Algorithm DeepTrace*.

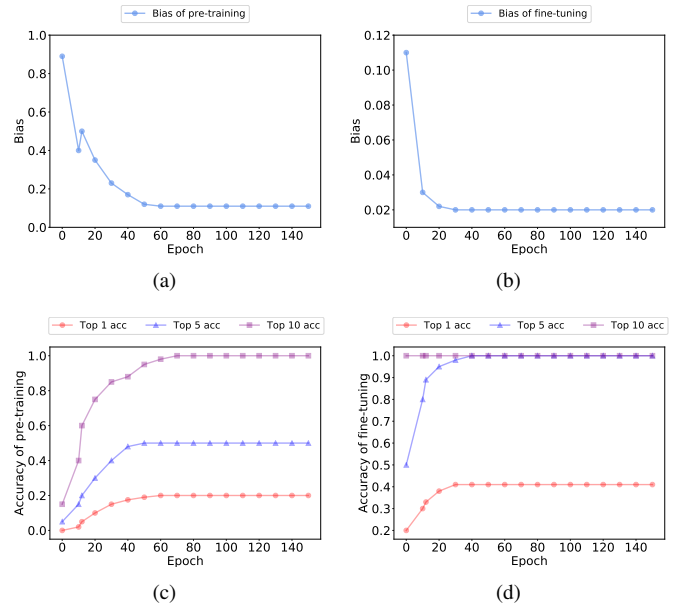


Fig. 6: Illustration of the results of the GNN model: (a) and (b) depict the bias trajectory between the approximate likelihood probability obtained by the GNN model and the accurate likelihood probability for the testing dataset during the pre-training and fine-tuning phases, respectively. (c) and (d) show the trajectories of top-1, top-5, and top-10 accuracies for the testing dataset during the pre-training and fine-tuning phases, respectively.

Among 1000 generated synthetic epidemic networks, we use 50% for pre-training, 25% for fine-tuning, and 25% for

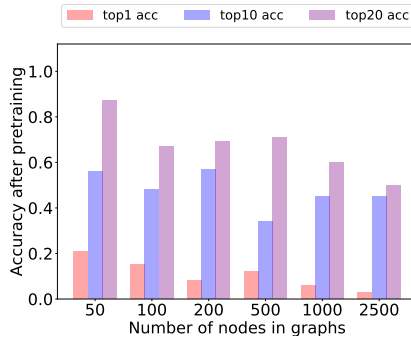


Fig. 7: The top-1, top-10, and top-20 prediction accuracies for validation datasets after pre-training in Algorithm DeepTrace.

testing. Correspondingly, these datasets have approximately 50 ~ 1000, 50, and 50 ~ 1000 infected nodes in the synthetic epidemic networks. We then construct the initial node features $\mathbf{h}_v^{(0)} = [\mathbf{1}, \hat{r}(v), \tilde{r}(v)]^T$ for each node in these networks according to the analysis in the previous section. For the training data used in the pre-training phase, we label each node with $\hat{\mathbb{P}}(G_n | v)$ in (11), while for the network data used in the fine-tuning phase and testing, we label each node with the exact probability $\mathbb{P}(G_n | v)$ in (2). A summary of these datasets is shown in TABLE I. Then we pre-train and fine-tune the GNN model in DeepTrace both for 150 epochs, and use the bias and a top- k accuracy to evaluate the performance of the trained model in the two-phase training process. The “top- k ” metric signifies that the trained GNN identifies the approximate superspreader as one of the k nodes with the highest probability of being superspreaders. This metric is similar to the `pass@k` metric for evaluating the functional correctness of code generated by pre-trained models in [45]. In particular, the `pass@k` metric is the probability that at least one of the top- k generated code samples for a problem passes the unit tests [45]. In the context of evaluating the efficacy of pre-trained models in learning to optimize, this metric measures how well the ranked nodes in G_n solves (1) based on the notion of network centrality. For example, if the approximate superspreader detected by the trained GNN is in the top-10 set, it indicates that this node is among the 10 most likely superspreaders. If it is in the top-1 set, it is the most likely superspreader. Thus, the lower the value of k in the top- k set, the higher the likelihood that the detected node is the most probable superspreader. Moreover, a higher likelihood of the optimal solution to (1) being among the top- k for a smaller k implies better performance of the pre-trained GNN. Thus, the “top- k ” metric effectively measures the frequency with which the global optimal solution of (1) appears within the top-ranked prediction outputs of the pre-trained GNN, offering a quantitative assessment of the accuracy in learning to optimize. The results are shown in Fig. 6.

Another key evaluation is to measure the generalizability of *DeepTrace Algorithm*, that is, to validate the effectiveness of the trained model by the small-scale epidemic networks in the larger epidemic networks. We construct six additional synthetic network validation datasets, each with 100 networks, and the number of nodes in each set of networks is

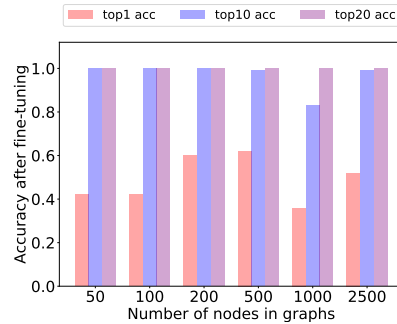


Fig. 8: Validation dataset accuracy metrics at top-1, top-10, and top-20 prediction levels after fine-tuning in Algorithm DeepTrace.

50, 100, 200, 500, 1000, and 2500, respectively. We use the SI model to simulate the spreading for a given number of infected nodes to generate the infection graphs (see Section IV-B). We then evaluate the performance of the trained GNN on these validation datasets using a metric based on top- k accuracy.

After training for 150 epochs, we evaluate the prediction accuracy at top-1, top-10, and top-20 for each validation dataset. The results of the pre-training and fine-tuning processes are illustrated in Fig. 7 and Fig. 8, respectively. Fig. 7 displays the accuracy trends during the pre-training phase, showing a steady improvement in performance as the model learns. In contrast, Fig. 8 depicts the fine-tuning phase results, highlighting how the model adjusts and refines its predictions with additional training. These figures collectively demonstrate that the training accuracy remains relatively stable, not deteriorating significantly even as the number of nodes in the epidemic networks increases. This indicates robust performance and adaptability of the GNN across varying network sizes. This phenomenon underscores the utility of developing data-driven models using small-sized networks for training, with the expectation that these models can generalize effectively to larger-sized networks. Utilizing smaller networks not only reduces overall training time but also facilitates leveraging transfer learning to extend models for superspreader detection in larger networks.

B. Evaluation on BFS and DFS tracing

In this section, we compare the performance of BFS and DFS tracing strategies using first detection time and average error as evaluation metrics, defined by equations (7) and (8), respectively. Here we take into account five groups of epidemic network datasets with distinct topological structure. The relevant statistics for these data are displayed in TABLE II. In the final column, we use d to represent the degree of the regular network, p to indicate the likelihood of edge formation between nodes in the ER random network, and $NC/p/q$ to denote the number of communities, the probability of edge formation within a community, and the probability of edge formation between communities, respectively. Additionally, we define the sensor network’s coverage area as *Area* and the communication range, denoted as *CR*, as the utmost distance between sensors that can form an edge. Let us describe the process of the simulation experiment. In synthetic networks, we first establish the underlying network \mathbb{G} using

different random network models. Next, based on the SI model described in Section II-A, we uniformly and randomly select a source node and begin simulating the spread of the virus on \mathbb{G} . Since the number of nodes in our real-world network data is around 100, we stop this spreading process once the number of infected nodes reaches 100, resulting in a 100-node epidemic network \mathbb{G}_N . To ensure fairness (as different index nodes may lead to significant performance differences), each node in \mathbb{G}_N is selected as the index node to start the contact tracing process.

We perform forward contact tracing using BFS or DFS and employ Algorithm DeepTrace along with two other methods, Rumor Center [15], and SCT [23], for backward contact tracing. As we expand the contact tracing network G_n , each time a new node is added, we compute the current estimated superspreader in G_n and measure the distance between this estimated superspreader and the true source, noting the error in hops at that moment (cf. (7)). When the estimated superspreader first corresponds to the true source, we record the current size of G_n as the first detection time. When $G_n = \mathbb{G}_N$, we will have identified 100 approximated superspreaders and their corresponding error hops. We calculate the average of these 100 error hops as the average error hops for this simulation experiment. This experiment is repeated hundreds of times on the same underlying network \mathbb{G} , but with different epidemic networks \mathbb{G}_N , recording the average error hops, first detection time, and the time spent. We initiate the contact tracing simulation directly on this data for the real-world network data (Taiwan and Hong Kong COVID-19 datasets), as these networks already represent epidemic conditions.

The theoretical result we obtained in Theorem 1 for the BFS strategy describe the distance between the approximated superspreader and the MLE, whereas the theoretical results, from Lemma 1 and Theorem 2, for the DFS strategy calculate the upper bound of the number of nodes that will be marked as approximated superspreaders during the contact tracing process. The theoretical results for BFS and DFS are entirely different in scope, so we cannot determine which strategy is better based on theory alone. In our simulation experiments, we tested six combinations of DeepTrace, Rumor Center, and STC with either BFS or DFS and recorded the first detection time in Table III and the average error in Table V. In addition, we also verify the results of Lemma 1 and Theorem 2 in Table IV. In Table III, we can observe that DeepTrace+BFS outperforms other methods from the first detection perspective. Additionally, within Rumor Center and STC, the BFS strategy generally outperforms the DFS strategy. On the other hand, from the perspective of average error, when the underlying network is a tree, DeepTrace+DFS performs better. Otherwise, DeepTrace+BFS is the best choice.

In addition to testing the performance of different methods on average error and first detection time, we also evaluated the computational efficiency of DeepTrace, Rumor Center, and STC. For computational efficiency, we recorded the time taken for contact tracing using DeepTrace, Rumor Center, and STC combined with DFS and BFS and calculated the average for DFS and BFS. As Table VI shows, DeepTrace's computational speed is significantly higher than that of the

other two methods.

C. DeepTrace for COVID-19 Epidemic Networks

In this section, we conduct experiments on COVID-19 pandemic data in Taiwan and Hong Kong to evaluate the performance of *Algorithm DeepTrace*. A summary of these epidemic network datasets is presented in TABLE VII. We refer to G_n as the epidemic network in the following, where nodes in G_n represent confirmed cases, and each edge in G_n implies that there is close contact between two confirmed cases. We compare *Algorithm DeepTrace* to estimators using (2), and since these two clusters are relatively small, the computation of the ML estimator (2) is feasible.

1) Contact Tracing for COVID-19 Pandemic in Taiwan:

The COVID-19 Omicron is a variant of the SARS-CoV-2 virus first reported on 24 November 2021, has shorter incubation times and is known to be more contagious than previous variants (with an effective reproduction number of 18.6 as compared to the Alpha variant of 3) that has since become the predominant variant in circulation worldwide. The infectiousness of Omicron has led to huge infection graphs and severely undermined the capacity of contact tracing in many countries. We first conduct experiments using data on the early spread of Omicron of COVID-19 in Taiwan from March 13, 2022, to April 1, 2022. The data is collected from the confirmed case reports released daily by the Taiwan Centers for Disease Control at <https://www.cdc.gov.tw>. Each node in the networks represents a confirmed case and is marked with the reported number of the confirmed case. Each edge represents a close contact between two confirmed cases.

Fig. 9 is the largest contact tracing networks constructed with the collected data with 92 confirmed cases. Case 22595 is the reported superspreader in this contact tracing network. As Case 22595 is also the earliest discovered case, we consider it as the index case for contact tracing. Using the trained GNN in Algorithm DeepTrace, we applied it to this network and detected that Case 22595, which is colored red, is the most likely superspreader. These findings align with the actual superspreaders reported by the Taiwanese authorities.

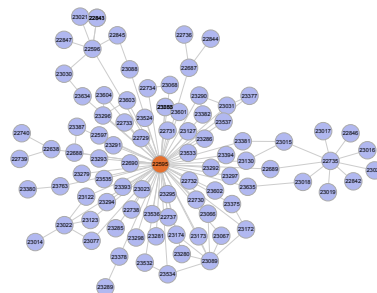


Fig. 9: Illustration of contact tracing with DeepTrace for a COVID-19 Omicron variant outbreak in Taiwan in early 2022. The blue nodes represent infected nodes, while the red nodes are the superspreaders predicted by DeepTrace, which incidentally correspond exactly to the actual superspreaders (i.e., ground truth) reported by the Taiwanese authorities.

Epidemic network	Underlying graph	$ \mathbb{G}_N $	Components	Other parameters
Complete N-ary graph	Nodes = 3500, Edges = 3499	100	1	$N = 3$
Regular tree	Nodes = 3500, Edges = 3499	100	1	$d = 3$
ER random graph	Nodes = 3500, Edges = 6016	100	1	$p = 10^{-3}$
SBM network	Nodes = 3500, Edges = 8086	100	1	$p = 5 \times 10^{-4}$, $q = 2 \times 10^{-4}$, $NC=3$
Sensor network	Nodes = 3500, Edges = 5710	100	1	Area= $55km^2$, CR= $130m$
Real-world network (Taiwan)	Nodes =92, Edges =117	92	1	–

TABLE II: Summary of the datasets used for performance comparison with BFS and DFS tracing.

Epidemic Network	DeepTrace		Rumor center		SCT	
	DFS	BFS	DFS	BFS	DFS	BFS
Complete N-ary graph	34.00	7.17	34.81	8.18	38.60	16.95
Regular tree	36.10	16.14	63.06	18.21	64.44	46.25
ER random graph	48.27	12.48	65.13	10.97	23.56	36.75
SBM network	34.07	47.14	49.03	54.98	44.56	40.7
Sensor network	32.47	18.71	33.45	21.14	39.28	36.75
Real-world network (Taiwan)	1.18	0.55	2.95	3.08	4.59	4.61

TABLE III: The average first detection time of DeepTrace and baseline methods across different types of epidemic networks, utilizing BFS and DFS tracing.

Epidemic Network	Forward tracing	DeepTrace			Rumor center			SCT		
		$\frac{ S_1 }{N-1}$	$\frac{ S_1 }{N-2}$	$\frac{ S_3 }{N-1}$	$\frac{ S_1 }{N-1}$	$\frac{ S_2 }{N-1}$	$\frac{ S_3 }{N-1}$	$\frac{ S_1 }{N-1}$	$\frac{ S_2 }{N-1}$	$\frac{ S_3 }{N-1}$
Complete N-ary graph	DFS	0.78	0.08	0.13	0.97	0.02	0.01	0.96	0.03	0.01
	BFS	0.88	0.08	0.04	0.97	0.02	0.01	0.98	0.02	0.00
Regular tree	DFS	0.66	0.21	0.13	0.91	0.06	0.03	0.89	0.07	0.04
	BFS	0.69	0.17	0.13	0.92	0.05	0.03	0.94	0.05	0.01
ER random graph	DFS	0.71	0.16	0.13	0.94	0.04	0.02	0.96	0.03	0.01
	BFS	0.79	0.11	0.10	0.95	0.03	0.02	0.96	0.03	0.01
SBM network	DFS	0.74	0.12	0.14	0.94	0.04	0.02	0.93	0.05	0.02
	BFS	0.83	0.08	0.09	0.95	0.03	0.02	0.96	0.03	0.01
Sensor network	DFS	0.76	0.14	0.10	0.94	0.04	0.02	0.94	0.04	0.02
	BFS	0.83	0.09	0.08	0.94	0.04	0.02	0.94	0.04	0.02
Real-world network (Taiwan)	DFS	0.87	0.07	0.06	0.97	0.02	0.01	0.97	0.02	0.01
	BFS	0.68	0.23	0.09	0.98	0.01	0.01	0.98	0.02	0.00

TABLE IV: Statistical analysis of consecutive pairs of approximated superspreader for DeepTrace and baseline methods across various types of epidemic networks employing BFS and DFS tracing. Note that the value of $\frac{|S_i|}{N-1}$ represents the percentage of $|S_i|$ in the total quantity, which is $|S_1| + |S_2| + |S_3|$.

Epidemic Network	DeepTrace		Rumor center		SCT	
	DFS	BFS	DFS	BFS	DFS	BFS
Complete N-ary graph	0.84	1.54	1.35	2.31	1.04	1.66
Regular tree	2.37	2.45	2.63	2.56	2.62	3.30
ER random graph	2.70	2.52	2.93	2.92	2.78	2.55
SBM network	2.55	2.30	2.78	2.86	2.73	2.69
Sensor network	2.67	2.61	3.50	3.42	3.06	2.85
Real-world network (Taiwan)	0.97	0.65	1.38	0.88	0.79	0.80

TABLE V: The average error during contact tracing for Algorithm DeepTrace and the baselines on various types of epidemic networks using BFS and DFS tracing strategies.

Methods	N = 64	N = 128	N=256	N=512
DeepTrace	0.58	5.83×10^1	7.39×10^2	1.12×10^3
Rumor center	2.32×10^1	4.36×10^2	1.03×10^3	2.52×10^4
SCT	4.32×10^1	6.55×10^2	6.22×10^3	1.43×10^5

TABLE VI: The efficiency comparison, in terms of time required (measured in seconds) for contact tracing, between Algorithm DeepTrace and other baseline methods across epidemic networks of varying scales.

2) Contact Tracing for COVID-19 Pandemic in Hong Kong:

As Hong Kong adhered to a strict ‘Zero-COVID’ policy with rigorous quarantine and testing measures, its population remained largely unaffected by the COVID-19 virus until January 2022. The introduction of the Omicron variant to this largely susceptible population led to one of the world’s highest death tolls in February and March 2022, despite Hong Kong’s early and widespread access to vaccines and the lower lethality of Omicron compared to previous variants [46], [47]. This unique situation, not previously observed in other parts of the world, presents a real-world scenario where the SI spreading model can be applied to evaluate the performance of Algorithm DeepTrace using training data from Hong Kong’s Omicron outbreak.

We first consider an epidemic network with four connected components in Hong Kong from 31 December 2021 to 22 January, the data for which is from [47]. This epidemic network contains 102 SARS-CoV-2 Omicron infections associated with four imported cases (nodes 1, 29, 70, and 100) in the connected components, which serve as ground truths of superspreaders. In this network, we use DeepTrace to iteratively identify the most likely superspreader as described by (2) as the forward contact tracing network expands. The illustration of the epidemic network and contact tracing process is depicted in Fig. 10. Initially, we select nodes 12, 36, 85, and 102 as the index cases and the starting points for the forward contact tracing process. As the contact tracing network grows, the most likely superspreader identified by DeepTrace shifts from node 12 to node 1, from node 36 to node 35 and finally to node 29, from node 85 to node 84 and finally to node 70, and from node 102 to node 100 in the four connected components, respectively. The final detected superspreaders (nodes 1, 29, 70, and 100) match the most likely superspreader given by (2) in the four connected components. Additionally, nodes 1, 29, and 100 are also the true superspreaders, while node 70 is just one hop away from the true superspreader, node 68. These results demonstrate that DeepTrace performs well in tracing the superspreaders.

Next, we consider utilizing DeepTrace on another epidemic network in Hong Kong where the ground truths of superspreaders are unknown. Following [46], we retrieved data of confirmed Omicron cases in Hong Kong from January 31, 2022, to February 3, 2022, from the Hong Kong government’s public sector open data portal at <https://data.gov.hk/en-data/dataset/hk-dh-chpsebceddr-novel-infectious-agent>. We used this data to construct epidemic networks, where each node represents a confirmed case and an edge connects two nodes if the cases were known to visit the same building at any time. We used the earliest reported case in [46] as the initial index case of the outbreak to

conduct forward contact tracing. Algorithm DeepTrace was then employed iteratively to identify the superspreaders as the contact tracing networks expanded.

Fig. 11 presents the contact tracing networks using the retrieved data, illustrating how the iterative outputs of DeepTrace eventually approaches the most likely superspreader given by (2) as the forward contact tracing network expands. For example, in the largest spreading cluster shown in Fig. 11, case 12611 is considered the index case and the initial superspreader. We initiate the forward contact tracing process from this case. As the contact tracing network grows, the most likely superspreader identified by DeepTrace shifts from case 12611 to case 12747, and finally to case 12825, which is exactly the most likely superspreader given by (2) in the entire epidemic network. Therefore, even without prior knowledge of the true superspreaders, DeepTrace can effectively identify the most likely superspreaders. By focusing treatment or implementing quarantine measures on these identified superspreaders, we may be able to suppress further propagation of the epidemic.

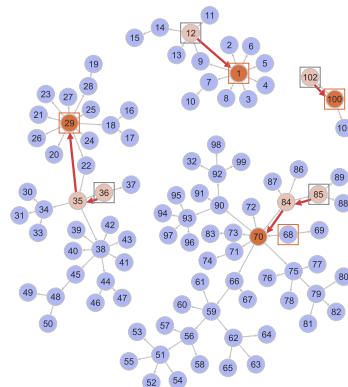


Fig. 10: Illustration of contact tracing with DeepTrace for an early Omicron outbreak in Hong Kong from 31 December 2021 to 22 January. The blue nodes represent infected nodes. The nodes in the gray boxes are considered the index cases of the Omicron outbreak. The nodes in the red boxes are the true superspreaders. The nodes in pink are superspreaders detected in the subgraph of the epidemic network during contact tracing. The nodes in red are the most-likely superspreaders in the spreading clusters in the epidemic network. The red arrows indicate the movement of superspreaders detected by DeepTrace as contact tracing continues.

VI. CONCLUSION

Digital contact tracing remains an open issue in tackling pandemics. In this paper, we have formulated the backward contact tracing problem as a maximum likelihood estimation of the epidemic source, which is crucial for identifying superspreaders in epidemic outbreaks. Given an index case, the contact tracer can explore the epidemic network using breadth-first search or depth-first search to compute the graph center of the instantaneous contact tracing subgraph, converging to the optimal likelihood estimate for certain graph topologies. We proposed Algorithm DeepTrace, which employs a graph neural network with semi-supervised learning, incorporating pre-training and fine-tuning phases for general and potentially large graphs through message passing. This approach is particularly beneficial for massive graph inference in computational epidemiology and is connected to online graph exploration,

Epidemic network	Nodes	Edges	Components	Ground truths	Avg. Error Hops to MLE	Avg. Err. Hops to ground truth
Taiwan (2022.03.13-2022.04.01)	92	117	1	Known	0	0
Hong Kong (2021.12.31-2022.01.22)	102	97	4	Known	0	1/4
Hong Kong (2022.01.31-2022.02.03)	402	390	11	Unknown	0	ground truth unknown

TABLE VII: A summary of COVID-19 epidemic network datasets for Algorithm DeepTrace.

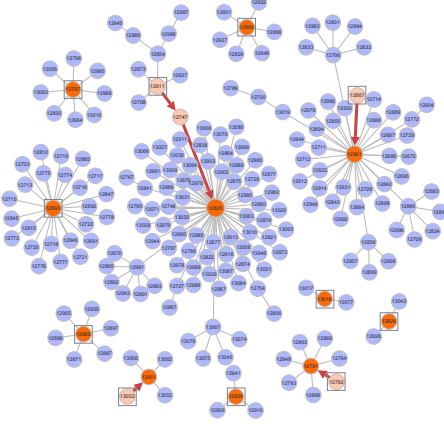


Fig. 11: Illustration of contact tracing using *Algorithm DeepTrace* for an early Omicron outbreak in Hong Kong in 2022. The blue nodes represent infected nodes. The nodes in the boxes are the index cases of the Omicron outbreak. The nodes in pink are superspreaders detected in the subgraph of the epidemic network during contact tracing. The nodes in red are the most-likely superspreaders in the spreading clusters in the epidemic network. The red arrows indicate the movement of superspreaders detected by DeepTrace as contact tracing continues.

whose maze-solving perspective offers promising avenues for contact tracing with low-complexity greedy algorithms. We validated the effectiveness of our methodology by modeling and analyzing real data from COVID-19 superspreading events in Hong Kong and Taiwan, demonstrating that our contact tracing algorithm can outperform existing heuristic methods.

To further enhance digital contact tracing, future work will focus on exploring advanced data-driven online graph exploration techniques and adaptive learning algorithms to handle dynamic and evolving epidemic networks. Additionally, we aim to find efficient decomposition techniques to break down the underlying optimization problem into smaller subproblems suitable for machine learning. Extending *Algorithm DeepTrace* to incorporate real-time data streams and improve scalability for larger networks will be crucial. Lastly, our approach, which focuses on learning to optimize contact tracing, can be refined and incorporated into scalable surveillance systems, enhancing the monitoring and mitigation of future pandemics.

APPENDIX

A. Proof of Theorem 1

Let \mathbb{G}_N be a d -regular tree and $\bar{v} \in \mathbb{G}_N$ satisfies (5), we assume that the maximum distance from \bar{v} to all leaves nodes is $k + 1$. Then by (5), there are only two possible distances from \bar{v} to all leaves, which are k and $k + 1$. For simplicity, let

$T_{d,k}$ denote the perfect d -regular tree with k levels, and we assume that the level of the root is 0. We denote t_v^u as the size of the subtree rooted at v after removing the edge $\{(u, v)\}$ from \mathbb{G}_N .

We have the following properties of \mathbb{G}_N :

- 1) The topology of \mathbb{G}_N is composed of $T_{d,k}$ plus some node v that satisfies $\text{dist}(\bar{v}, v) = k + 1$ and v is connected to a leaf node in $T_{d,k}$, moreover, we have $\bar{v} = v_N^*$.
- 2) If \bar{v} is the root of \mathbb{G}_N , then all subtree of \mathbb{G}_N satisfy (5).

The proof of the above two properties can be found in the following subsections. Since \mathbb{G} is a d -regular tree, finding the superspreader by (2) is equivalent to finding its centroids [17], i.e., v_n^* is the centroid of \mathbb{G}_N . Let \bar{v} be the root of \mathbb{G}_N , then we can prove Theorem 1 by showing that if $v_i^* \neq v_{i+1}^*$, then v_{i+1}^* is the parent of v_i^* . To contrary, assume $\exists i < N$ such that $v_i^* \neq v_{i+1}^*$ and $v_{i+1}^* = v_c$, where v_c is a child of v_i^* . Without loss of generality, we can assume that v_i^* is at the l th level of \mathbb{G}_N . Then, from the above property 1, we can deduce that $t_{v_c}^{v_i^*} > t_{v_i^*}^{v_c}$ since v_c is the centroid of \mathbb{G}_N . Note that the maximum size of $t_{v_c}^{v_i^*}$ is $\frac{(d-1)^{k-l+1}-1}{d-2}$ since the subtree rooted at v_c also satisfies (5) by the above property 2. Similarly, since the BFS algorithm discovers all vertices at a distance $k-l$ from v_i^* , we have the minimum size of $t_{v_i^*}^{v_c} = (d-2) \frac{(d-1)^{k-l}-1}{d-2} + \frac{(d-1)^{k-l}-1}{d-2} + 1$, where the first term of this equation is the sum of the size of all other subtrees rooted at v_i^* except the one rooted at v_c . The second term is the size of $t_{v_p}^{v_i^*}$ where v_p is the parent of v_i^* , and the third term is v_i^* itself. Hence, we have $t_{v_c}^{v_i^*} = t_{v_i^*}^{v_c}$ which contradicts the assumption that the v_c is the centroid of \mathbb{G}_N . We can conclude that v_{i+1}^* must be the parent of v_i^* if $v_i^* \neq v_{i+1}^*$ which implies that the trajectory of v_n^* is the shortest path to the root $v_N^* = \bar{v}$.

B. Proof of Property 1 of \mathbb{G}_N used in Theorem 1

Let \mathbb{G}_N be a d -regular tree and $\bar{v} \in \mathbb{G}_N$ satisfies (5), we assume that the maximum distance from \bar{v} to all leaves nodes is $k + 1$. Then by (5), there are only two possible distances from \bar{v} to all leaves, which are k and $k + 1$. By the definition of d -regular tree and (5), we can deduce that for all $v \in \mathbb{G}_N$ $\text{dist}(v, \bar{v}) < k$, v is not a leaf of \mathbb{G}_N which implies the degree of v must be d . Hence, \mathbb{G}_N contains a d -regular tree with k levels denoted as $T_{d,k}$. The rest of the nodes in $\mathbb{G}_N \setminus T_{d,k}$ are leaves in \mathbb{G}_N with distance k or $k + 1$ from the node \bar{v} . Since the topology of \mathbb{G}_N is composed of $T_{d,k}$ and an additional leaf-level, we can conclude that $\bar{v} = v_N^*$ [10], [17].

C. Proof of Property 2 of \mathbb{G}_N used in Theorem 1

Let \mathbb{G}_N be a d -regular tree and $\bar{v} \in \mathbb{G}_N$ satisfies (5), we assume that the maximum distance from \bar{v} to all leaves nodes is $k+1$. Let \bar{v} be the root of \mathbb{G}_N , and $v \in \mathbb{G}_N$ be an arbitrary node. If v is a leaf or the root of \mathbb{G}_N , then the subtree rooted at v satisfies (5).

If v is not a leaf or the root of \mathbb{G}_N , then we prove this property by contradiction. Assume that the subtree rooted at v , denoted as $T_v^{\bar{v}}$ does not satisfy (5), then there are two leaves $u, w \in T_v^{\bar{v}}$, satisfy $|\text{dist}(u, v) - \text{dist}(w, v)| > 1$. since \mathbb{G}_N is a tree, we have $\text{dist}(\bar{v}, u) = \text{dist}(\bar{v}, v) + \text{dist}(v, u)$ and $\text{dist}(\bar{v}, w) = \text{dist}(\bar{v}, v) + \text{dist}(v, w)$ which implies $|\text{dist}(\bar{v}, u) - \text{dist}(\bar{v}, w)| > 1$ and contradicts to our assumption.

D. Proof of Theorem 2

We can prove this theorem by showing that if $(v_{j_1}^* = v, v_{j_1+1}^* = u) \in S_2$ and $(v_{j_2}^* = v, v_{j_2+1}^* = w) \in S_2$ where $j_2 > j_1$, then we have $j_2 > 2j_1$. Assume there are two pairs $(u, v), (w, v) \in S_3$ where $u, v, w \in \mathbb{G}_N$. Since each pair in S_3 must have a corresponding pair in S_2 , there are $(v_{j_1}^* = v, v_{j_1+1}^* = u) \in S_2$ and $(v_{j_2}^* = v, v_{j_2+1}^* = w) \in S_2$. If we treat the index case v^1 as the root of \mathbb{G}_N , then we have $v_{j_1}^*$ is the parent of $v_{j_1+1}^*$ and $v_{j_2}^*$. Let u be the d_1 th node and w be the d_2 th node visited by the DFS strategy respectively, i.e., $v_{j_1+1}^* = v^{d_1}$ and $v_{j_2+1}^* = v^{d_2}$ where $d_2 > d_1$.

Note that if a node in \mathbb{G}_N with weight strictly less than $n/2$, then the node is the unique ML estimator on contact tracing network \mathbb{G}_N [15]–[17]. Hence we have

$$j_1 + 1 = 2d_1 - 1.$$

Moreover, since $(v = v_{j_2}^*, v_{j_2+1}^*) \in S_2$, we have

$$\begin{aligned} j_2 + 1 &= 2d_2 - 1 \\ &> 2(j_1 + 1) - 1 \\ &= 2j_1 + 1. \end{aligned}$$

The second inequality follows by $d_2 > j_1 + 1$ since w will not be visited until the subtree $T_u^v \subseteq \mathbb{G}_N$ is fully visited by the DFS algorithm. We can conclude that if v is involved in more than one pairs say (u, v) and $(w, v) \in S_3$ then there are corresponding pairs $(v = v_{j_1}^*, u = v_{j_1+1}^*)$, and $(v = v_{j_2}^*, w = v_{j_2+1}^*) \in S_2$ in S_2 with index $j_2 > 2j_1$. From Lemma 1, we have $|S_2| \leq (N-1)/2$, which implies v cannot be involved in more than $\log_2 \frac{N-1}{2}$ pairs in S_3 , since each pair $(u, v) \in S_3$ must have a corresponding $(v, u) \in S_2$.

E. Proof of Lemma 1

Since the DFS contact tracing starts from the index case v^1 , we can assume that the index case v^1 is the root of the DFS tree. Now, we are able to distinguish parent-node and child-node in each pair $(v_j^*, v_{j+1}^*) \in S$. Due to the property of the DFS tracing, a node is fully visited when all its descendants are fully visited; we have the following observation: If $(v_j^* = u, v_{j+1}^* = v) \in S_2 \cup S_3$ and v is the parent of u , then there is no other $i > j$ such that $(v_i^* = v, v_{i+1}^* = u) \in S_2 \cup S_3$. Moreover, we can observe that:

1) If $(u, v) \in S_2$, then u is the parent node of v .

2) If $(u, v) \in S_3$, then u is the child of v .

Since the estimated superspreader changes from u to v only when $P(\mathbb{G}_N | v) > P(\mathbb{G}_N | u)$. We can conclude that both type two and type three transitions must be followed by a type one transition, which means the size of the type one transition is more than type two and type three. Hence, we have $|S_1| \geq |S_2| + |S_3|$. Moreover, from the above two properties, we have the fact that for each $(u, v) \in S_3$, there is a corresponding $(v, u) \in S_2$, i.e., $|S_2| \geq |S_3|$. Combining the results above, we have $|S_1| \geq |S_2| \geq |S_3|$.

Since $|S_1| + |S_2| + |S_3| = N - 1$ and $|S_2| \geq |S_3|$, we can deduce that $|S_1| \geq \frac{N-1}{2}$ and $|S_3| \leq \frac{N-1}{4}$.

F. Proof of Theorem 3

As shown in (2), solving MLE problem needs the information of all the permitted permutations for all the nodes in G_n . Since a newly infected node can only be infected by one of its infected neighbors, v_{i+1} must be the neighbor of v_i in any permitted permutation σ , and thus calculating $p(\sigma | v)$ with (4) is actually a recursive process of aggregating the information of degree $d(v_l)$ and Φ_l from the l th layer's neighbors of node v in σ , which can be expressed as

$$\mathbb{P}^{(l)}(\sigma | v) = \sum_{u \in N_G(v)} f(\mathbb{P}^{(l-1)}(\sigma | v), \mathbb{P}^{(l-1)}(\sigma | u)), \quad (12)$$

with $\mathbb{P}^{(l)}(\sigma | v)|_{l=1} = 1/d(v)$. Therefore, it is a recursive iteration to calculate $\sum_{\sigma \in \Omega(G_n|v)} \mathbb{P}(\sigma|v)$ to aggregate the information of degree $d(v_l)$ and Φ_l from its l th layer's neighbors in all $\sigma \in \Omega(G_n | v)$, which can be shown as

$$\begin{aligned} &\mathbb{P}^{(l)}(G_n | v) \\ &= \sum_{\sigma \in \Omega(G_n|v)} \sum_{u \in N_G(v)} f(\mathbb{P}^{(l-1)}(\sigma|v), \mathbb{P}^{(l-1)}(\sigma|u)) \\ &= \sum_{u \in N_G(v)} g(\mathbb{P}^{(l-1)}(G_n|v), \mathbb{P}^{(l-1)}(G_n|u)). \end{aligned} \quad (13)$$

Note that (13) demonstrates the process of iterative aggregation to calculate $\mathbb{P}(G_n | v)$ for node v . Since \mathbb{G} is connected, the shortest distance between any two nodes satisfies $\text{dist}(u, v) \leq \text{diam}(G)$. Thus, after a number of $\text{diam}(G)$ steps of aggregation and combination, each node can obtain the feature information of all nodes in the graph. Furthermore, it is evident that both $f(\cdot)$ and $g(\cdot)$ are continuous functions. Consequently, based on the universal approximation theorem, these functions can be approximated to any desired degree of precision using standard multilayer perceptrons with hidden layers and non-constant, monotonically increasing activation functions [42].

REFERENCES

- [1] S. Landau, *People Count: Contact-Tracing Apps and Public Health*. MIT Press, 2021.
- [2] Y. Bengio, P. Gupta, T. Maharaj, N. Rahaman, M. Weiss, T. Deleu, E. B. Muller, M. Qu, P.-I. St-charles, O. Bilaniuk *et al.*, "Predicting infectiousness for proactive contact tracing," in *Proceedings of the International Conference on Learning Representations (ICLR)*, 2021.
- [3] D. Leith and S. Farrell, "A measurement-based study of the privacy of Europe's COVID-19 contact tracing apps," in *Proceedings of the IEEE International Conference on Computer Communications*, 2021.

- [4] H. Stevens and M. B. Haines, "Tracetogether: pandemic response, democracy, and technology," *East Asian Science, Technology and Society*, vol. 14, no. 3, pp. 523–532, 2020.
- [5] Z. Fei, Y. Ryznyk, A. Sverdlov, C. W. Tan, and W. K. Wong, "An overview of healthcare data analytics with applications to the COVID-19 pandemic," *IEEE Transactions on Big Data*, vol. 8, no. 6, pp. 1463–1480, 2022.
- [6] D. C. Adam, P. Wu, J. Y. Wong, E. H. Y. Lau, T. K. Tsang, S. Cauchemez, G. M. Leung, and B. J. Cowling, "Clustering and superspreading potential of SARS-CoV-2 infections in Hong Kong," *Nature Medicine*, vol. 26, no. 11, pp. 1714–1719, 2020.
- [7] G. Cencetti, G. Santin, A. Longa, E. Pigani, A. Barrat, C. Cattuto, S. Lehmann, M. Salathe, and B. Lepri, "Digital proximity tracing on empirical contact networks for pandemic control," *Nature Communications*, vol. 12, no. 1, pp. 1–12, 2021.
- [8] S. Kojaku, L. Hébert-Dufresne, E. Mones, S. Lehmann, and Y.-Y. Ahn, "The effectiveness of backward contact tracing in networks," *Nature Physics*, vol. 17, no. 5, pp. 652–658, 2021.
- [9] W. J. Bradshaw, E. C. Alley, J. H. Huggins, A. L. Lloyd, and K. M. Esvelt, "Bidirectional contact tracing could dramatically improve COVID-19 control," *Nature Communications*, vol. 12, no. 1, pp. 1–9, 2021.
- [10] D. Shah and T. Zaman, "Rumors in a network: Who's the culprit?" *IEEE Transactions on Information Theory*, vol. 57, no. 8, pp. 5163–5181, 2011.
- [11] N. Bailey, *The Mathematical Theory of Infectious Diseases and Its Applications*. Hafner Press, 1975.
- [12] N. C. Grassly and C. Fraser, "Mathematical models of infectious disease transmission," *Nature Reviews Microbiology*, vol. 6, no. 6, pp. 477–487, 2008.
- [13] Y.-C. Chen, P.-E. Lu, C.-S. Chang, and T.-H. Liu, "A time-dependent SIR model for COVID-19 with undetectable infected persons," *IEEE Transactions on Network Science and Engineering*, vol. 7, no. 4, pp. 3279–3294, 2020.
- [14] R. Eletreby, Y. Zhuang, K. M. Carley, O. Yağan, and H. V. Poor, "The effects of evolutionary adaptations on spreading processes in complex networks," *Proceedings of the National Academy of Sciences of the United States of America*, vol. 117, no. 11, p. 5664, 2020.
- [15] D. Shah and T. Zaman, "Rumor centrality: a universal source detector," in *Proceedings of ACM SIGMETRICS/PERFORMANCE joint international conference on Measurement and Modeling of Computer Systems*, 2012.
- [16] B. Zelinka, "Medians and peripherians of trees," *Archivum Mathematicum*, vol. 4, no. 2, pp. 87–95, 1968.
- [17] P. D. Yu, C. W. Tan, and H. L. Fu, "Averting cascading failures in networked infrastructures: Poset-constrained graph algorithms," *IEEE Journal of Selected Topics in Signal Processing*, vol. 12, no. 4, pp. 733–748, 2018.
- [18] C. W. Tan and P.-D. Yu, "Contagion source detection in epidemic and infodemic outbreaks: Mathematical analysis and network algorithms," *Foundations and Trends in Networking*, vol. 13, no. 2-3, pp. 107–251, 2023.
- [19] L. Vassio, F. Fagnani, P. Frasca, and A. Ozdaglar, "Message passing optimization of harmonic influence centrality," *IEEE Transactions on Control of Network Systems*, vol. 1, no. 1, pp. 109–120, 2014.
- [20] N. Karamchandani and M. Franceschetti, "Rumor source detection under probabilistic sampling," in *Proceedings of the IEEE International Symposium on Information Theory (ISIT)*, 2013.
- [21] Z. Wang, W. Dong, W. Zhang, and C. W. Tan, "Rumor source detection with multiple observations: Fundamental limits and algorithms," in *Proceedings of the ACM SIGMETRICS Performance Evaluation Review*, 2014.
- [22] W. Luo, W. P. Tay, and M. Leng, "Identifying infection sources and regions in large networks," *IEEE Transactions on Signal Processing*, vol. 61, no. 11, pp. 2850–2865, 2013.
- [23] P.-D. Yu, C. W. Tan, and H.-L. Fu, "Epidemic source detection in contact tracing networks: Epidemic centrality in graphs and message-passing algorithms," *IEEE Journal of Selected Topics in Signal Processing*, vol. 16, no. 2, pp. 234–249, 2022.
- [24] A. Sridhar and H. V. Poor, "Sequential estimation of network cascades," in *Proceedings of the Asilomar Conference on Signals, Systems, and Computers*, 2020.
- [25] E. A. Meiron, C. Milling, C. Caramanis, S. Mannor, S. Shakkottai, and A. Orda, "Localized epidemic detection in networks with overwhelming noise," in *Proceedings of the 2015 ACM SIGMETRICS International Conference on Measurement and Modeling of Computer Systems*, 2015.
- [26] A. Sridhar and H. V. Poor, "Bayes-optimal methods for finding the source of a cascade," in *Proceedings of the IEEE International Conference on Acoustics, Speech, and Signal Processing*, 2021.
- [27] P.-D. Yu, C.-W. Tan, L. Zheng, and C. Zhao, "Unraveling contagion origins: Optimal estimation through maximum-likelihood and starlike tree approximation in markovian spreading models," *CoRR*, vol. abs/2403.14890, 2024. [Online]. Available: <https://arxiv.org/abs/2403.14890>
- [28] V. La Gatta, V. Moscato, M. Postiglione, and G. Sperli, "An epidemiological neural network exploiting dynamic graph structured data applied to the COVID-19 outbreak," *IEEE Transactions on Big Data*, vol. 7, no. 1, pp. 45–55, 2020.
- [29] C. Shah, N. Dehmamy, N. Perra, M. Chinazzi, A.-L. Barabási, A. Vespignani, and R. Yu, "Finding patient zero: Learning contagion source with graph neural networks," *arXiv preprint arXiv:2006.11913*, 2020.
- [30] X. Ru, J. M. Moore, X.-Y. Zhang, Y. Zeng, and G. Yan, "Inferring patient zero on temporal networks via graph neural networks," *AAAI*, vol. 37, no. 8, pp. 9632–9640, 2023.
- [31] S. Chen, P.-D. Yu, C. W. Tan, and H. V. Poor, "Identifying the superspreader in proactive backward contact tracing by deep learning," in *Proceedings of the 56th Annual Conference on Information Sciences and Systems (CISS)*, 2022.
- [32] A. Ganesh, L. Massoulie, and D. Towsley, "The effect of network topology on the spread of epidemics," in *Proceedings IEEE 24th Annual Joint Conference of the IEEE Computer and Communications Societies.*, vol. 2, 2005, pp. 1455–1466 vol. 2.
- [33] B. Awerbuch and R. Gallager, "A new distributed algorithm to find breadth first search trees," *IEEE Transactions on Information Theory*, vol. 33, no. 3, pp. 315–322, 1987.
- [34] S. Even, *Graph Algorithms*. Cambridge University Press, 2011.
- [35] B. Kalyanasundaram and K. Pruhs, "Constructing competitive tours from local information," *Theoretical Computer Science*, vol. 130, pp. 125–138, 1994.
- [36] N. Megow, K. Mehlhorn, and P. Schweitzer, "Online graph exploration: New results on old and new algorithms," *Theoretical Computer Science*, vol. 463, pp. 62–72, 2012.
- [37] H. Dai, Y. Li, C. Wang, R. Singh, P.-S. Huang, and P. Kohli, "Learning transferable graph exploration," *Proceedings of the 33rd International Conference on Neural Information Processing Systems (NIPS'19)*, no. 226, pp. 2518–2529, 2019.
- [38] I. Chiotellis and D. Cremers, "Neural online graph exploration," *arXiv preprint arXiv:2012.03345*, 2020.
- [39] T. N. Kipf and M. Welling, "Semi-supervised classification with graph convolutional networks," in *Proceedings of the International Conference on Learning Representations (ICLR)*, 2016.
- [40] W. L. Hamilton, Z. Ying, and J. Leskovec, "Inductive representation learning on large graphs," 2017.
- [41] Y. LeCun, Y. Bengio, and G. Hinton, "Deep learning," *Nature*, vol. 521, no. 7553, pp. 436–444, 2015.
- [42] K. Hornik, "Approximation capabilities of multilayer feedforward networks," *Neural networks*, vol. 4, no. 2, pp. 251–257, 1991.
- [43] P.-D. Yu, C. W. Tan, and H.-L. Fu, "Rumor source detection in finite graphs with boundary effects by message-passing algorithms," in *Proceedings of the 2017 IEEE/ACM International Conference on Advances in Social Networks Analysis and Mining 2017*, ser. ASONAM '17. New York, NY, USA: ACM, 2017, pp. 86–90.
- [44] A. A. Hagberg, D. A. Schult, and P. J. Swart, "Exploring Network Structure, Dynamics, and Function using NetworkX," in *Proc. of the 7th Python in Science Conference*, 2008, pp. 11 – 15.
- [45] M. Chen, J. Tworek, H. Jun, Q. Yuan, H. P. de Oliveira Pinto, J. Kaplan *et al.*, "Evaluating large language models trained on code," *arXiv:2107.03374*, 2021.
- [46] R. Xie, K. M. Edwards, D. C. Adam, K. S. M. Leung, T. K. Tsang, S. Gurung, W. Xiong, X. Wei, D. Y. M. Ng, G. Y. Z. Liu, P. Krishnan, L. D. J. Chang, S. M. S. Cheng, H. Gu, G. K. H. Siu, J. T. Wu, G. M. Leung, M. Peiris, B. J. Cowling, L. L. M. Poon, and V. Dhanasekaran, "Resurgence of Omicron BA.2 in SARS-CoV-2 infection-naïve Hong Kong," *Nature Communications*, vol. 14, p. 2422, 2023.
- [47] Y. M. Mefsin, D. Chen, H. S. Bond, Y. Lin, J. K. Cheung, J. Y. Wong, S. T. Ali, E. H. Lau, P. Wu, G. M. Leung *et al.*, "Epidemiology of infections with SARS-CoV-2 Omicron BA. 2 variant, Hong Kong, January–March 2022," *Emerging infectious diseases*, vol. 28, no. 9, p. 1856, 2022.